Chemical Physics 517 (2019) 253–264

Contents lists available at ScienceDirect

Chemical Physics

journal homepage: www.elsevier.com/locate/chemphys

Molecular dynamics on laccase from *Trametes versicolor* to examine thermal stability induced by salt bridges

Leonardo David Herrera-Zúñiga[a,b], Cesar Millán-Pacheco[c], Gustavo Viniegra-González[d], Elba Villegas[e], Leticia Arregui[f], Arturo Rojo-Domínguez[f,*]

[a] Área de Biofisicoquímica, Departamento de Química, Universidad Autónoma Metropolitana, Unidad Iztapalapa, San Rafael Atlixco No. 186, Col. Vicentina, Iztapalapa, C.P. 09340, Ciudad de México, Mexico
[b] Tecnológico de Estudios Superiores del Oriente del Estado de México, División de Estudios de Posgrado e Investigación, Paraje San Isidro s/n, Barrio de Tecamachalco, La Paz, Estado de México, C.P. 56400, Mexico
[c] Facultad de Farmacia, Universidad Autónoma del Estado de Morelos, Av. Universidad No. 1001, Col. Chamilpa, Cuernavaca, Morelos, C.P. 62209, Mexico
[d] Departamento de Biotecnología, Universidad Autónoma Metropolitana, Unidad Iztapalapa, San Rafael Atlixco No. 186, Col. Vicentina, Iztapalapa, C.P. 09340, Ciudad de México, Mexico
[e] Centro de Investigación en Biotecnología-UAEM, Av. Universidad 1001, Col. Chamilpa, Cuernavaca, Morelos, C.P. 62209, Mexico
[f] Departamento de Ciencias Naturales, Universidad Autónoma Metropolitana, Unidad Cuajimalpa, Av. Vasco de Quiroga 4871, Col. Santa Fe Cuajimalpa, C.P. 05348, Ciudad de México, Mexico

ARTICLE INFO

Keywords:
Thermostability
Fungal laccase
Molecular dynamics simulations
Cluster analysis
Electrostatics
MMPBSA

ABSTRACT

Enzymes have demonstrated their capacity to acquire thermostability with precise single-residue mutations. We developed a methodology to propose and evaluate stabilizing salt-bridge interactions into the structure of laccase. This oxidoreductase folds into three similar and interacting immunoglobulin-like domains. We identified structural positions prone to strengthen interdomain contacts with a single salt bridge. Ten mutated enzymes were modeled, along with positive and negative controls. We evaluated the mutated structures at three temperatures, with 153 molecular dynamics simulations. Results demonstrated that a computational methodology combining triplicates of molecular dynamics, Poisson-Boltzmann electrostatics and clustering based in principal component analysis, is robust and reliable. Arginine mutants were better than lysine to confer thermostability, and the results indicated that the complex network of interactions in a protein structure requires this type of combined approach to assess the effects of mutations.

1. Introduction

Structure is crucial for biological function. Both experimental and computational efforts have been performed in order to propose mutations to enhance stability of protein molecules. This improved stability allows the use of mutated protein molecules in technological applications where conditions are far from the natural environment of the bioactive molecule. Analysis of enzymes from mesophilic and thermophilic organisms has identified several general contributors to structural stabilization [1]. For example, some contributors are larger hydrophobic cores [2,3], additional polar interactions including hydrogen bonding [4–6], structural rigidity [7,8], glycosylation [2,4], and frequently an increased number of salt bridges [9–12]. With respect to computational efforts, molecular dynamics simulations (MD) and force field energy-calculations are two of the most frequently used tools in the search for thermostability, since the former allows estimation of the structural effects of potentially relevant mutations and the latter is a comparative criterion to contrast the mutant with the wildtype structure [13,14].

The inclusion of salt bridges in proteins is one of the strategies to enhance thermostability. Salt bridges are interactions between residues supporting opposite charges that are close enough (< 4 Å) to experience the attraction. These interactions are relevant for thermostable proteins because they represent plausible modifications that can be done on the surface of the protein to increase rigidity and decrease free energy [15]. They can be studied by experimental approaches like p*K*a perturbation and mutant productions. In the former case, the relative free energy gained or lost when ionizable groups are protonated is followed by an atom-resolution technique such as NMR. With mutant species, the coupling free energy between interacting charges is obtained by a double mutant cycle [16]. Force field energy, Poisson-Boltzmann calculations or molecular dynamics simulations, alone or in

* Corresponding author.
E-mail address: arojo@correo.cua.uam.mx (A. Rojo-Domínguez).

https://doi.org/10.1016/j.chemphys.2018.10.019
Received 19 June 2018; Received in revised form 24 September 2018; Accepted 27 October 2018
Available online 28 October 2018
0301-0104/

combination are some of the computational approaches to understand the effect of salt bridges over proteins [17,18]. Force fields evaluate the energy based on the atom coordinates of a structure; Poisson Boltzmann-based simulation uses a more complex electrostatic model with different dielectric constants for protein and solvent at each simulation temperature; and MD follows the effect of a new salt bridge over the original protein structure [19]. Addition of a salt bridge to a protein is reasonably expected to be a stabilizing interaction, but in the complex environment of the protein, it could result in neutral or negative effects. A robust and sensible method to predict when salt bridges will result in protein stability is a relevant goal in protein design.

Laccases are oxidoreductases used by some organisms like fungi to degrade the polyphenolic structure of lignin in wood as part of its digestion. Also, plants and other organisms use laccases in anabolic pathways to synthesize phenolic metabolites. These enzymes are widely used in industrial processes which require strong oxidative reactions like fabric color treatments, biomass processing for biofuel production, bioremediation of wastes in water and soils, etc. [20–24] and also for biosynthesis *in vitro* [25]. These usages require laccase activity over a wide range of salinity, pH and temperature. The molecular geometry of this group of enzymes is composed of three structural domains which share a common cupredoxin-like topology [26] similar to an immunoglobulin fold. This fold is formed by a beta sandwich composed by 8–12 antiparallel strands, with a complex connectivity going from one of the sheets to the other and a significant and well defined hydrophobic core [27]. Only the C-terminus structural domain maintains its capacity to shelter a copper ion, while the arrangement of the three domains forms a new binding site for a complex structure of three copper ions coordinated to eight histidine residues coming from the first and last domains. This assembly makes interdomain interactions crucial to maintaining copper binding and thus its oxidoreductase activity.

In this work, we propose a methodology to evaluate structural stability induced by mutations which produce ion pairs, isolated from other contributors to stability. The methodology centers on the analysis of data from MD simulations to get molecular information [28]. Laccase was used as a test case due to its importance in industrial and biological processes and also because of its three-domain structure. Since each domain is a well-packed structure, we tested the effect of interdomain salt bridges induced by point mutations in the energetics of the mutant structures and compared them with structures used as positive and negative controls.

2. Methods

2.1. Modeling and analysis

Homology modeling of wild-type and the 11 mutants of *Trametes versicolor (Tv)* laccase (See Table 1 and Fig. S1 in the Supplementary data) was performed with the Molecular Operating Environment package (MOE, www.chemcomp.com) [29] using PDB file 1GYC as a template. We initially started with 33 *Trametes versicolor* single-point mutants able to potentially form interdomain salt bridges. All of them were then energy minimized yielding 10 of them with energies below that of the wtTv laccase structure. The eleventh mutant (E142A) was generated as a negative control by a single-point mutant removing an existing interdomain salt-bridge. On the other hand, as a positive control, the wildtype β-glucosidase was taken from PDB file 2O9P, and its H62R thermostable mutant was also modeled with MOE. Another positive control was built from wildtype *Bacillus subtilis* laccase and its two mutants (E188K/R) were modeled using Modeller [30] package, with CotA laccase PDB ID:1GSK used as a template. Interface contacts were estimated with the PDBsum server (www.ebi.ac.uk/pdbsum) [31]. The acronyms used throughout this work are summarized in the Table S1 in the Supplementary data.

2.2. System setup and simulation protocols

All molecular dynamics simulations were performed using NAMD2.7 package [32] and CHARMm (toppar C22/CMAP parameters) [33] with a time step of 1 fs. Bonded hydrogen atoms were constrained with SHAKE algorithm as implemented in NAMD2.7. Long-range electrostatics was treated with Ewald particle mesh model. A 10-Å switch and 12-Å cutoff for non-bonded interactions were used, as employed for parameterization, and the non-bonded list was updated every 25 steps. Periodic boundary conditions with isotropic molecule-based scaling were applied. Berendsen temperature coupling method [34] was used to efficiently couple the system to a thermal bath and maintain the system close to the target temperature to approximate the simulation to an isothermal-isobaric ensemble.

In every one of the 17 structures studied, the system was built with CHARMM-GUI (http://www.charmm-gui.org/) [35]. All systems were solvated with TIP3P water in a rectangular box that extended to at least 1 nm between the protein and the edge of the box involving about 24 thousand water molecules, in a physiological solution of KCl (0.15 mol L^{-1}, Table S2). Basic and acid residues were protonated at pH = 7.0 on each of our models and simulations. All crystallographic waters from PDB files were conserved.

Previous to each MD simulation all solvated systems were energy minimized with NAMD2.7 with 50,000 steps of conjugate gradient algorithm. MD runs were carried out to simulate 20–30 ns, and consistently only the last 5 ns of each simulation were used for analysis [36,37], storing snapshots every ps. A total of 153 runs were performed, counted as 17 different species (eleven mutants of *Trametes versicolor* laccase, two mutants CotA of *Bacillus subtilis* laccase and one of β-glucosidase, and the three corresponding wildtype structures). For each of the mutant structures and all three wild-type reference structures, we carried out MD simulations at 298.15 K, by triplicate [38]. Similar simulations were performed at 323.15 K and 348.15 K, also by triplicate. In short, we performed nine runs (three for each temperature) on each of the 17 structures (3 wt and 14 mutants) for a total of 153 independent simulations.

2.3. MM/PBSA approach

The free energies of wild-type *Trametes versicolor* laccase (wt*Tv*), *Bacillus subtilis* laccase (wt*Bs*), bacterial *β-glucosidase* B (wt*β*glu) and their mutants were calculated with the MM/PBSA methodology [38] using CHARMm (version 35b2). Briefly, the free energy of each conformation sampled from MD simulation is expressed as a potential of mean force W. It is calculated as the sum of the *intramolecular energy of the protein* (U) and a solvation free energy term that is further split in polar (ΔG^{polar},electrostatic) and nonpolar ($\Delta G^{nonpolar}$,hydrophobic) terms [39], described in the Eq. (1).

$$\bar{W} = U(\bar{r}_1, \cdots, \bar{r}_n) + \Delta G^{polar}(\bar{r}_1, \cdots, \bar{r}_n) + \Delta G^{nonpolar}(\bar{r}_1, \cdots, \bar{r}_n) \quad (1)$$

All structures were previously energy-minimized to remove high energy spots, like van der Waals clashes, with all atoms in the structure unrestrained. Then a more accurate solvent model (the generalized Born solvent-accessible model) was used in order to reduce artifacts caused by the missing solvent. The entropy of the protein is neglected altogether here based on the assumption frequently made that the entropy of similar compact conformations is practically the same [39,40]. Since we deal in this work with changes due to single-point mutant structures, their comparative change is expected to be small. The polar energy (ΔG^{polar}) has been computed according to the Poisson-Boltzmann theoretical framework as the difference in free energy for a hypothetical charging process of the solute *in vacuo* and in ionic solvent. Grid spacing was set to 0.5 Å, and the longest linear dimension of the grid was extended to at least 20% beyond the protein. Parse radii were employed for all atoms [41]. Pauling van der Waals radii by ions were used

Table 1
Description of enzyme mutants of wt*Tv* (11 mutants), wt*Bs* (2 mutants), and wt*β*glu (1 mutant).

	Mutant	Partner	Mutation location	Partner location	Interacting domains and line colors in Fig. 1B
Mutants of wt*Tv*	A184D	ARG22	*β*-turn connecting sheet C and D	2nd strand of sheet A	B:A orange, right
	A184R	ASP18		*β*-harping between 1st and 2nd strands in sheet A	B:A gray, right
	A497D	LYS59	14th helix	*β*-turn between 1st helix and 2nd strand in sheet B	C:A black/white, right
	A71K A71R	ASP444	*β*-turn connecting 2nd strand in sheet B and helix two	γ-turn between 6th strand in sheet B and 4th strand in sheet G	A:C pink, left
	A88K A88R	ASP498	*β*-turn between 2nd helix and 4th strand in sheet A	14th helix	A:C cyan, right
	G175R	ASP18	between 2nd strand in sheet C and 5th strands in sheet D	*β*-harping 1st and 2nd strands in sheet A	B:A light green, right
	L158R	ASP23	*β*-harping between 1st and 2nd strands in sheet C	2nd strand in sheet A	B:A magenta, right
	L308E	ASP136	*β*-turn between 7th helix and 1st strand in sheet E	16th helix	C:A purple, left
	E142A[#]	ARG37	5th helix	1st strand in sheet B	B:A green, left
Mutant of wt*Bs*	E188K[*] E188R[*]	ASP14 GLU61	1st and 4th strand of sheet A		
Mutant of wt*β*glu	H62R[*]	GLU429	4th helix	last strand in sheet D	

Mutant and partner residues constitute salt-bridge interactions. Negative and positive control mutants were identified by [#] and [*], respectively. Color code for lines in Figs. 1 and 3 are given in the last column. Location of these positions with respect to secondary structure elements can be followed in Fig. 3. Right or left indicate the localization of the color line in Fig. 1B.

according to the force field. The value of the exterior dielectric constant was set according to the run temperature (78.54 at 298.15 K, 69.94 at 323.15 K and 62.69 at 348.15 K), and the solute dielectric constant was set to 2.0 in the three temperatures [42]. The same-type of ions and salt concentration were used for each DM run. Non-polar solvation energy ($\Delta G^{nonpolar}$) is proportional to the solvent-accessible surface area (SASA) $\Delta G^{nonpolar} = \gamma SASA + \beta$, where the surface tension coefficient γ has been taken equal to 0.00542 kcal (mol^{-1} $Å^{-2}$) and β = 0.92 kcal mol^{-1} [43]. Note that MM/PBSA free energies reported hereafter are extremely large because they are given relative to a non-physical reference state, but the relevant figures for our work rely on comparative analysis between a wild-type and a mutant species, turning irrelevant the reference state, and yielding reasonable energy amounts.

2.4. Cluster energy approach

The ensemble of snapshots obtained from an MD simulation in principle approximates to a thermodynamic ensemble. Theoretical and numerical inaccuracies of both MD and PBSA methodologies, however, lead to some fluctuations in the computed MM/PBSA energy. The cluster energy approach proposed by Schulten K. et al. [44] was applied to gather representative states and filter some outlier structures. The principal component analysis approach was developed to reveal the most important motions in wildtype and mutant enzymes according to the protocol established by Sengupta et al. [45]. A conformational search is carried out through cartesian Principal Component Analysis (PCA) by generating clusters of all the snapshots that are close structurally to each other in an RMSD cutoff of 2.4 Å using Carma Software [46]. The effectiveness of principal component analysis (PCA) is a widely established technique for finding global and correlated motions in atomic simulations develop by MD simulations [47,48]. This study was carried out using the first three principal components generated through Carma, obtaining the most populated clusters, the RMSD cutoff used as a measure of the center of each cluster was 2.4 Å. The probability distribution between the first two principal components was made on the alpha carbon atoms. The free energy (ΔG) is calculated according to Eq. (2), assuming a Boltzmann distribution of previously obtained populations [46].

$$\Delta G = -k_b T \ln\left[\frac{P}{P_{max}}\right] \quad (2)$$

In the Eq. (2), k_b is Boltzmann's constant, T the temperature in absolute units, and P over P_{max} is the ratio between the probability obtained from the distribution of the first two principal components and the maximum probability, respectively [46].

All simulations were performed at the LANCAD (Laboratorio Nacional de Cómputo de Alto Desempeño) at the Laboratorio de Supercómputo y Visualización en Paralelo (LSVP), from the Universidad Autónoma Metropolitana, Unidad Iztapalapa (UAM-I, Mexico). The analysis was performed using scripts written in home with CHARMm version 35b2 and Simulaid programs [33,49]. Visual analysis of protein structures was carried out using VMD [50]. The copper ions on the active site of laccase enzyme were modeled declaring and using collective variables (COLVAR module [51]) on NAMD, and their parameters were taken from Lowell W. et al. [52]. The general flow chart of the methodology is depicted in the Supplementary Fig. S1.

3. Results and discussion

For homology modeling, we used the 519 aa sequence of *Trametes versicolor* fungal laccase from gene lac1 as expressed by Lopez et al. [53], with GenBank accession number AY049725.1. Homologous sequences from the Protein Data Bank were searched with BLAST, and 1GYC was located. Although 1GYC lacks the first 20 residues of AY049725.1, in the rest of its sequence it is a closely-related homolog, with 97% identity also from *T. versicolor* fungus, and with no indels in the sequence alignment. Homology model building was based on the 499 aa of 1GYC as a template, replacing 15 residues on it (Supplementary Table S3): ten of them on external sites, three conservative changes in the interior of the first two domains, and two conservative and correlated changes in the interdomain region of these two domains. The overall RMS distance of alpha carbons between 1GYC and the homology model (wt*Tv*) of our sequence was 0.4 Å, indicative that side chain replacements produced no significant structural changes.

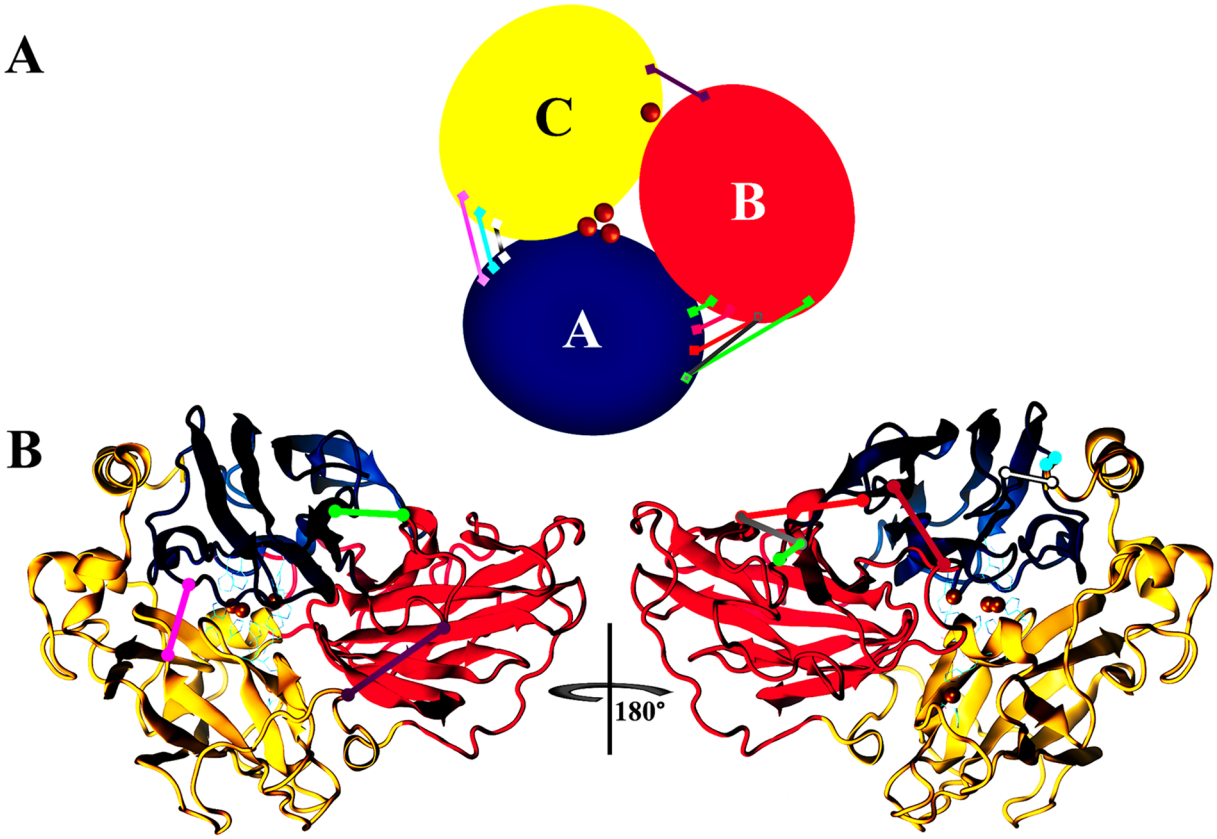

Fig. 1. Structure of *T. versicolor* laccase. A. Depiction of wt*Tv* domains represented with large ellipses, and the schematic location of copper ions shown by brown spheres. Lines correspond to the salt bridges generated by single point mutations (see Table 1 for full-color code). Since two different salt bridges occur in the same place with A71R and A71K mutations, they are represented by the same pink line, as well as A88R and A88K by the same cyan line, so only 8 lines appear for the 10 salt bridges studied. The deleted salt bridge in the negative-control mutation E142A is also depicted (green). B. Ribbon structure of wt*Tv* showing the location of all salt bridges introduced, shown as a color line joining the α-carbons of participating residues. The salt bridge deleted in the negative control is also shown as a green line at left.

3.1. Mutant design

Each one of the three domains in laccase chain (designated from now on as A, B, and C) has a similar compact immunoglobulin-like fold, composed of a beta sandwich and loops of variable length, with several of them connecting strands of different sheets (Fig. 1). This fold has been named as cupredoxin-like and is characterized in the CATH superfamily 2.60.40.420 with more than 2200 domains known [54]. Due to its complex topology and tight packing, this type of domain is difficult to unfold; therefore to propose the location of potentially stabilizing salt-bridges, we focused our analysis on the interdomain contacts of laccase. So, we compared the domain-domain contacts in laccase with interdomain or interchain interfaces of similar size proteins. For example, those between papain left and right domains (9PAP), between the C- and *N*-termini domains of human complement D (5MT4), and also with the interchain contacts in triosephosphate isomerase (7TIM) homodimer (Supplementary Table S4). Comparatively, *T. versicolor* laccase interdomains present a reduced number of hydrogen bonds and non-bonded contacts when compared with the other molecules, especially in comparison with other thermotolerant and thermostable laccases. The structural characteristics of the wt*Tv* laccase along with the idea that even partial disruption of interdomain contacts ineludibly would affect activity, led us to propose that one of the best sites for introducing stabilizing salt-bridges would be between contiguous side chains from different domains. Care was also taken to avoid alteration of the oxidoreductase due to the introduction of the new salt-bridge interactions, so they were proposed on the surface of the enzyme far from the multicopper site and also from the water channel where water molecules produced during catalytic cycles are released [55].

To propose the location of the stabilizing salt bridges, we analyzed the wt*Tv* structure to identify acid or basic residues in the structure, adjacent to an electrically neutral side chain in a contiguous domain. Table 1 shows a list of single point mutations of those electrically neutral residues able to produce salt bridges with potential stabilizing effect on interdomain interactions. In this work we propose and studied a total of 10 mutations creating salt bridges (color lines in Fig. 1), along with four reference structures to be used to validate our results; one of them was a mutation which deletes an already existing interdomain salt-bridge in *T. versicolor* laccase (E142A), as a negative control (Fig. 1). In contrast, as positive controls we also studied three salt-bridge mutants reported to induce thermostability: one in bacterial *β*-glucosidase (H62R) increasing denaturation temperature in about 3.0 °C [56,57] and two in *Bacillus* sp. laccase (E188K and E188R). During analysis, each control mutant was compared to its corresponding wild-type structure, denoted herein as wt*Tv,* wt*β*glu and wt*Bs*, respectively. Regarding the wt*Bs* mutants, the increased thermal stability of laccase from *Bacillus* HR03 was found by site-directed point mutations of E188 replacing this residue two times by two positive residues (Lys and Arg). The E188K variant was stabilized by 5 °C, while E188R mutation showed a moderate stability improvement compared to the wt*Bs* [58].

3.2. Molecular dynamics simulations

Starting from wt*Tv* structure, we constructed all 11 mutants (10 potentially stabilizing and the negative control) by homology modeling. The *Bacillus subtilis* wild-type and its mutants E188K and E188R were built using Modeller [30] utilizing as template CotA laccase, with PDB

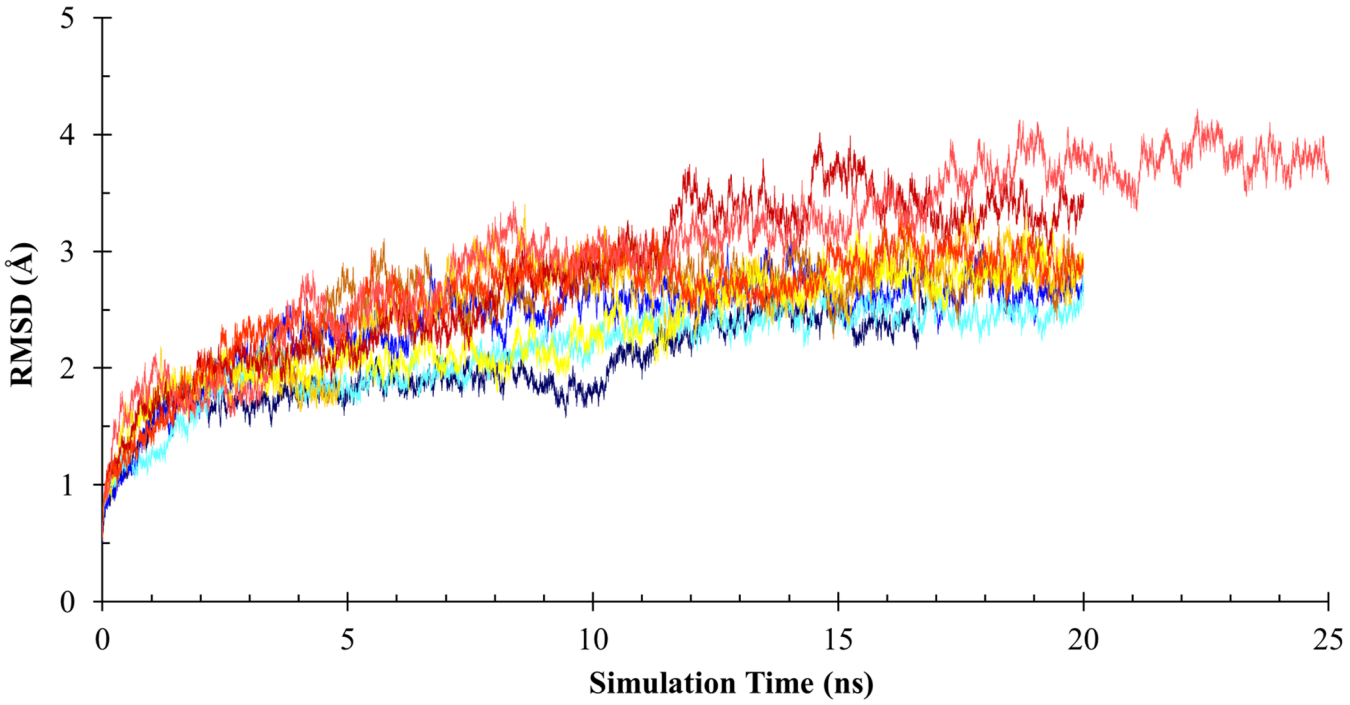

Fig. 2. Alpha carbon RMSD of molecular dynamics simulations of A71R mutant. Blue, yellow and red hues correspond to triplicated runs at 298.15, 323.15 and 348.15 K, respectively. Equivalent figures for the rest of the mutants and the wildtype structures are included in the Supporting information as Figs. S2–S5. All runs were carried out at pH 7.0 and 0.15 mol L^{-1} of KCl.

code 1GSK. Also, we used the crystallographic structure of wt*β*glu reported in the PDB (code 2O9P) and modeled its thermostable H62R mutant. The simulations on all 17 structures (14 mutants and 3 wt references, Table 1) required up to 10 ns to reach stability, and most of our runs were 20 ns long. All runs were carried out at pH 7.0 with an ionic strength of KCl 0.15 mol L^{-1}. Fig. 2 shows a typical RMSD evolution on time of alpha carbons for the nine runs of A71R mutant of *T. versicolor* laccase, it shows the typical process to attain thermal equilibrium of the system. The equivalent figures for wild-type species and the rest of the mutant structures are included as Supporting information (Supplementary Figs. S2–S5). To allow for proper equilibration and to test the steadiness of simulations, some MD simulations were allowed to run more than 20 ns, finding a stable behavior. The entire set of 153 MD runs sums more than 3.1 μs of MD simulation. To be consistent in the data collection from the runs, in all cases only the last 5 ns of simulation were used for further analysis, comprising 5000 snapshots at 1 ps intervals for each simulation. Remarkably, the intensity of RMSD fluctuations during simulations, like those shown for A71R in Fig. 2, were somewhat higher than we expected, and also higher than those obtained for wt*β*glu and also for its H62R mutant. This behavior was consistent with the runs for all laccase mutants (108 in total), but in our experience, it is worth analyzing its origin as indicative of structural information [59]. We compared the amplitude of RMSD and fluctuations in the equilibrium region of the DM with the equivalent reported for other systems (dimeric or multimeric proteins) and laccases simulations [4,60]. Since laccase is structurally organized in packed domains, it is expected that its RMSD values approach those from the relative movement of chains in multimeric proteins [61–64]. Since we did not use fixed copper atoms but used a tethering scheme by COLVAR (see Methods) we diagnosed a less packed structure in the internal interdomain region of the laccase structure, attributed to higher fluctuation in simulations of this enzyme, both from *T. versicolor* and *B. subtilis* and from other previously published MD simulations of laccases [4,60]. Noteworthy, this comparative analysis of MD trajectories gave us indirect confidence in the equilibrium conditions of the runs analyzed in this work.

To further validate that our results correspond to a reasonable description of the molecular system, we compared the RMS-fluctuations at three different temperatures for each amino acid of wt*Tv*, averaged in three independent replicas, with the experimental B-factor in 1GYC (Fig. 3). Also, we submitted all laccase mutants to the Elastic Network Model, as implemented in elNémo server (http://www.sciences.univ-nantes.fr/elnemo) [65], to have an independent estimation of the local chain flexibility as predicted B-factor (Fig. S6). We found a satisfactory qualitative correlation between data from computational and experimental sources and our simulation, at the three simulated temperatures. We also observed repeatability in our results; and as expected, higher fluctuations were observed with higher temperature. It is evident from this figure that the first two domains have most of the highest fluctuating regions, which occur mainly in loop regions connecting secondary structure elements. Most of the potential stabilizing interactions are located precisely between these two domains. Also, it can be seen that copper ions are located in relatively rigid segments.

3.3. Salt-bridge stabilization

With the aim of estimating the effect of mutations, MM/PBSA energy was calculated for each of the 5000 snapshots collected during the last 5 ns of the simulations (Fig. 4). This procedure was also performed for each of the three replicas in each of the runs. All traces in Fig. 4 show fluctuations around a constant value, although they did not reach precisely the same average energy value, as a consequence of the random assignment of velocities inherent to MD simulations. This is a typical result of MD indices when replicas of the same molecular system and simulation parameters are performed as has been previously described [30,66]. However, MM/PBSA energies for A71R at 348.15 K (red hues in Fig. 4) tend to be higher than those from simulations at 298.15 K (blue hues) with intermediate values for the middle temperature. This comparative result is similar in all simulations for wt and mutant species and shows that during simulations at higher temperatures interactions are somewhat weaker than at lower temperature, due to a broader structural fluctuation. To compare the structural stability of mutants respect to

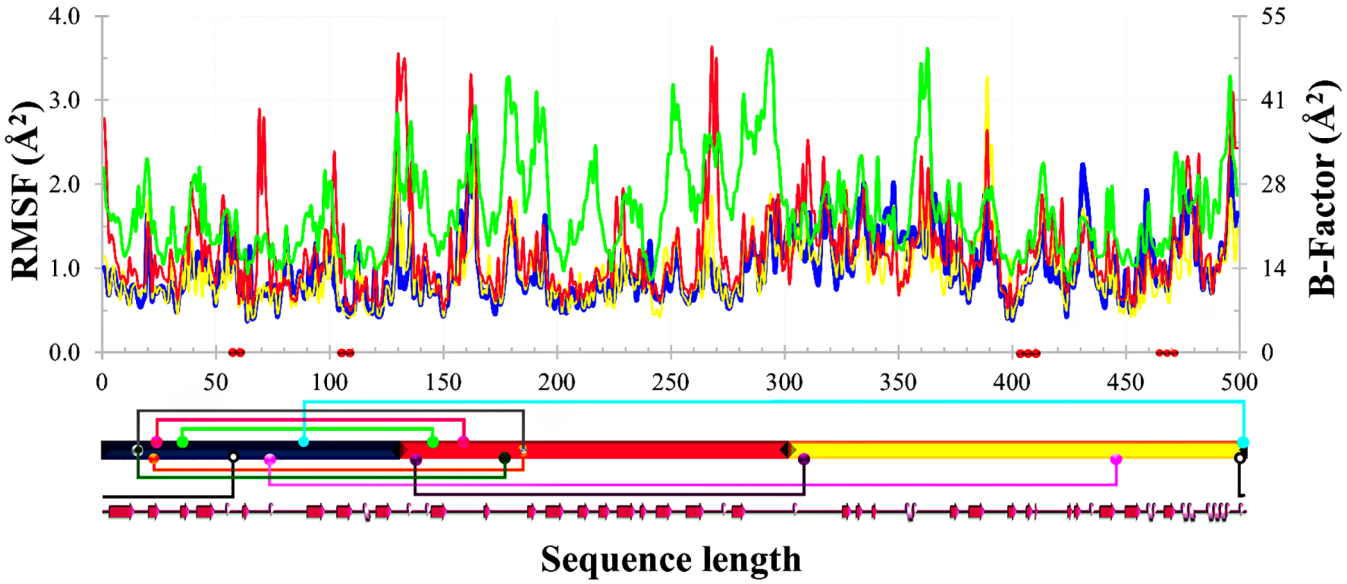

Fig. 3. Local fluctuation of wt*Tv* during MD simulations. Comparisons of RMS fluctuations in simulations to B-factors from crystallized laccase (green line) are represented for the three runs averaged at 298.15 (blue), 323.15 (yellow) and 348.15 K (red). Residues interacting with copper ions are shown on the *x* axis with a brown circle. The extent of domains A, B and C are indicated with the bar in blue, red and yellow, respectively. Along with this bar, color lines describe the studied salt bridge interactions, with the same color code of Table 1 and Fig. 1. At the bottom, secondary structure elements along the wt*Tv* sequence are shown: beta strands with magenta arrows and helices in white. An equivalent comparison of our MD simulations to fluctuations calculated by elNémo is shown in Fig. S6 of Supplementary data.

wildtype, the set of 15,000 energy values from each triplicate of MD simulations was averaged at each temperature, and the average from the respective wildtype MD runs was subtracted (*i.e.,* wt*Tv*, and also wt*Bs* and wt*βglu* for the positive controls). Energy differences are presented in Fig. 5 for the ten different mutants and for the positive and negative controls (Table S5). Negative values denote a stabilized structure with respect to the wt reference, while positive results indicate that the mutation affected its molecular environment in a destabilizing way. As expected for positive control, wt*β*glu and wt*Bs* are stabilized by H62R, E188K, and E188R mutations respectively. On the other hand, the E142A negative control for laccase is destabilized. Interestingly mutations of wtTv show a variety of behaviors. Several of the salt bridges demonstrated were destabilizing, and most mutations incorporating arginine residues were the most promising to confer thermostabilization.

Further analysis of these results showed that averaging data from three different runs might mask some of the effects, such as fluctuation of data and divergence between runs presented in Fig. 4. Also, averaged data in Fig. 5 for 323.15 K (yellow points) are not intermediate respect to the extreme temperatures. Results from these two figures encouraged us to find a different mode of data analysis. Exploring details of the snapshots obtained during the runs, and comparing mutant to wildtype conformations, made evident that some common structural characteristics were repeatedly visited during simulations. To gather and classify such structural features, the set of structures collected during each replica of MD simulations was submitted to a clustering algorithm. The wt*Tv*, wt*Bs* laccases and *β*-glucosidase are composed of 7495, 8090 and 7052 atoms (N), respectively, about half of them are hydrogen atoms restricted by the SHAKE algorithm, so during dynamics simulations,

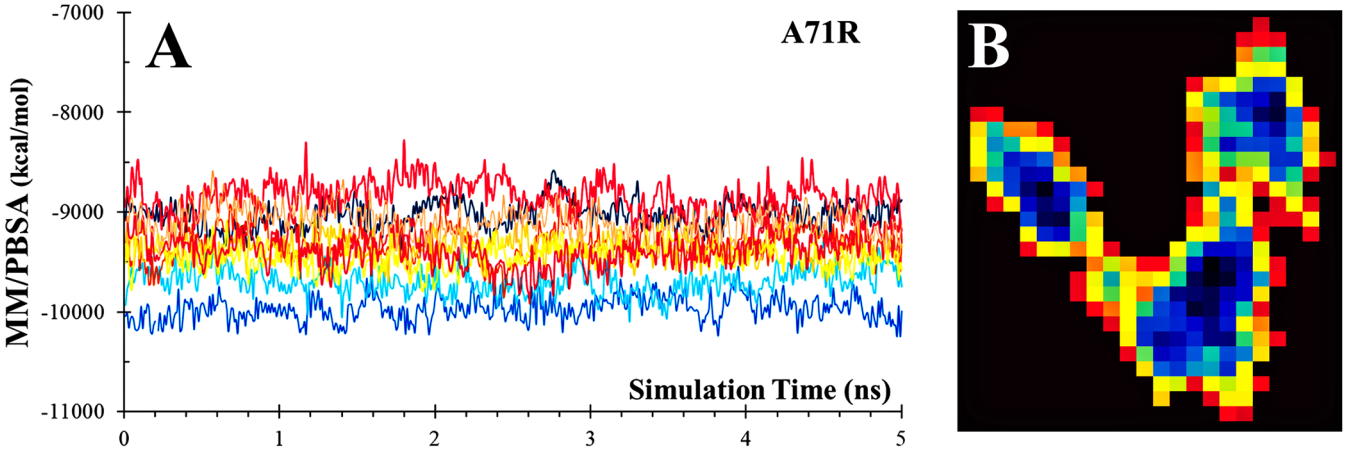

Fig. 4. A. Time evolution of electrostatic energy for the A71R mutant. Blue, yellow and red hues correspond to the three replicas of runs at 298.15, 323.15 and 348.15 K, respectively, as in Fig. 2. Equivalent figures for the rest of the structures are included in the Supporting information (Fig. S7–S10). Although energies are calculated with respect to an arbitrary reference state, this state becomes irrelevant when canceled by subtraction of wt to a mutant structure. B. Example of clustering of one of the runs of A71R. Vertical and horizontal axes are the two most significant principal-components, determined from structural characteristics of the 5000 snapshots taken from one of the three MD simulations for this mutant. Dark blue colors represent the higher population of structures. In this case, the set of snapshots was classified into three main groups of similar structures, or clusters.

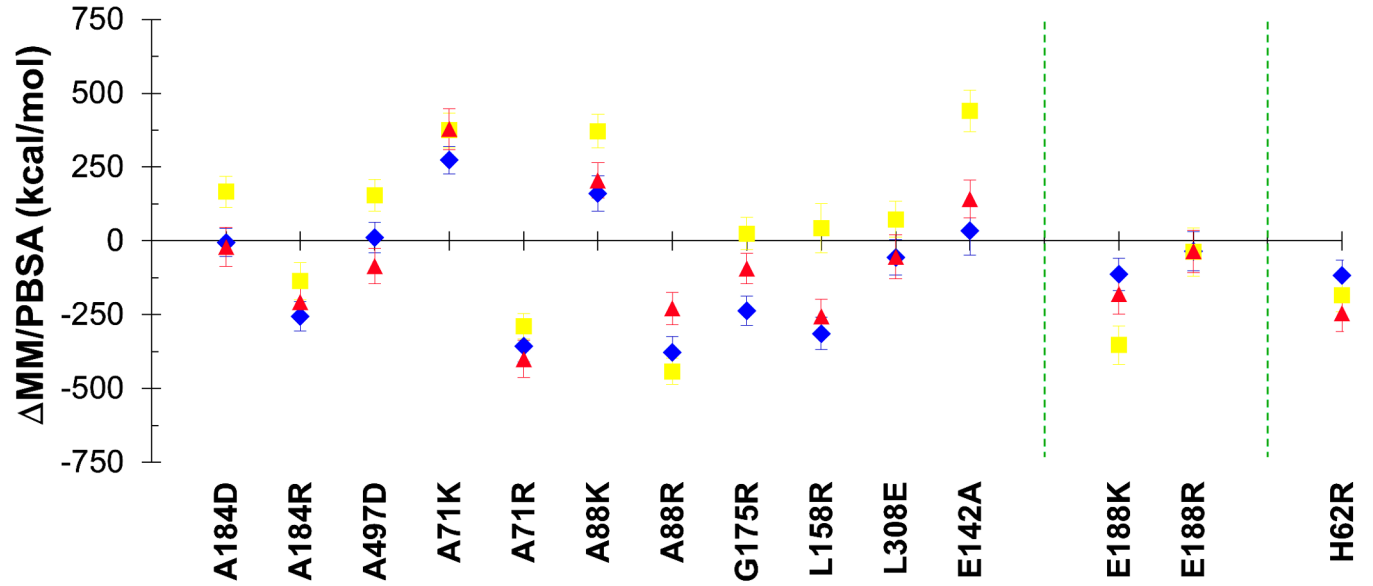

Fig. 5. Stabilizing effect of mutants. Average energy from simulations of mutants with respect to the average energy from their corresponding wildtype structure. Each mutation is represented at the three temperatures studied 298.15 (blue), 323.15 (yellow) and 348.15 K (red), and includes snapshot averages over the three replicas of MD simulations. E142A corresponds to a negative control on wt*Tv*. E188K and E188R correspond to positive controls on wt*Bs*, and H62R to a positive control of wtβglu.

only half of the atoms of the proteins were actually free to move independently. The 3 (N/2) degrees of structural freedom were transformed by a principal components analysis, and the two most representative abstract eigenvectors (or abstract principal components) were used to classify the similar structures from each of the 153 runs, into typically two or three clusters (Fig. 4B). Therefore, each cluster is formed by a set of similar structures from an MD simulation with significant divergences to those in other clusters of the same run. An archetypal structure for every cluster is selected, representing all the structures of that set. Then the energy and conformation of all archetypes of mutant clusters were compared to each one from its wildtype clusters. Differences in energy between mutant and wildtype archetypal structures, as well as the RMSD between them, are plotted in Fig. 6, at the three different temperatures assayed (filled points). Each of these points is the comparison between the representative structure of a cluster for a mutant and that of a cluster from its corresponding wildtype structure.

3.4. Mutant structures are similar to their wt

From the complex set of data collected at 298.15 K shown in Fig. 6A we can identify the yellow points corresponding to the positive control of H62R mutant of β-glucosidase respect to wtβglu. They segregate at the lower left zone of the diagram, (low RMSD values) meaning that mutation in this enzyme stabilized the structure (as reported experimentally) and did not cause significant changes in its structure. Regarding the other positive controls, clusters from E188K, E188R mutants of *Bs*-laccase were compared to those of wtBs. The E188K and E188R clusters have a behavior similar to H62R mutation; the points corresponding to the two *Bs*-laccase mutants are located mainly in the negative energy zone, too. However, the structure of Lys mutant shows an RMSD closer to wild-type enzyme compared to Arg mutant. The positions of E188K, E188R, and H62R in the negative energy zone signify that mutations stabilized the structures of wt*Bs* and wtβglu respectively, as expected for positive control. The negative control points (green) are located mainly at right, as a result of a significant structural perturbation caused by the mutation. Its position above the zero energy line is a consequence of the loss of a salt bridge, thus destabilizing the structure. The average RMSD values are 1.46, 1.53, 1.31 and 1.69 Å for H62R, E188R, E188K, and E142A controls at 298 K, respectively; while differences in energy are −154 (± 105), −144 (± 124), −253 (± 93) and +47 (± 61) kcal/mol, for positive controls and negative controls. Although Lys mutant of wt*Bs* have a stabilizing behavior, it is of lower magnitude than in the Arg mutant. The rest of the filled points corresponds to cluster-comparison results from the remaining 10 *Tv*-laccase mutants. Cluster data collation in Fig. 6 is accessible on Table S6. Blue points are closer to the yellow ones showing a stabilizing behavior for most of the mutants introducing an arginine residue. In contrast, cyan points are nearer the negative control indicating that lysine is not stabilizing the structure. Red points correspond to mutants introducing acid side chains, and show intermediate positions. The right panel presents the averages calculated from all the points of the same mutant, representing an alternative view of the same relative distribution. It is interesting to note that some of the charged residues introduced in wt*Tv* laccase resulted in destabilizing salt bridges. This type of destabilizing charged residue has been reported for other laccase mutants, for example replacing an aspartate side chain for a proline promotes stabilization of the structure [67].

3.5. Basic residues in wtTv

We designed two pairs of mutants where an arginine or a lysine is inserted in the same position: one pair is A71R and A71K, and the other is A88R and A88K. Although arginine is slightly larger than lysine, the distance from the alpha carbon to the center of the positive electric charge is almost the same. Nevertheless, strong divergences were aroused in the stabilizing effect in each pair. This is graphically seen in Fig. 6A where mutants with arginine residues (blue) are systematically situated in lower energy regions than mutants where lysine was inserted (cyan). This same behavior is observed at the three temperatures studied. Arginine side chains showed a higher probability of stabilizing electrostatic-interactions than lysine during the MD simulation. Comparative analysis of cluster-representing structures from MD simulations demonstrates that the distance to the partner in the salt bridge is smaller than in the case of arginine than in lysine and shows lower fluctuations (Fig. 7). Although the same formal charges are involved in each of these salt bridges, it has been experimentally demonstrated by mass spectrometry that charge density is a significant factor for domain

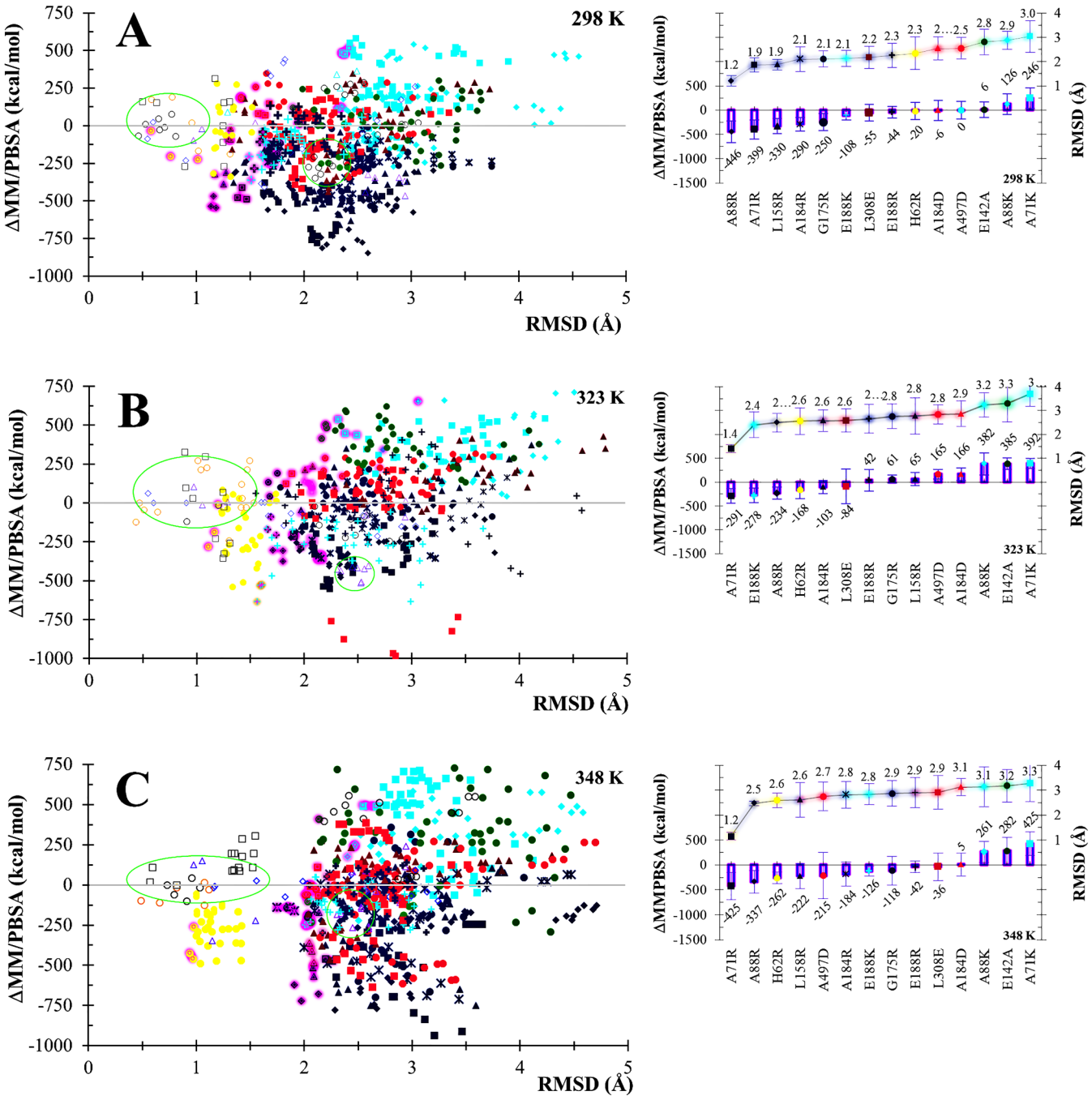

Fig. 6. Energetic and structural comparison of clusters. Left. Each point corresponds to a comparison between the archetypal structure of a cluster from a mutant and one of its corresponding wild-type structures. The vertical axis is the energy difference between the representative structures of the pair of clusters compared, while the horizontal axis is their structural difference expressed as RMSD. Each color stands for one type of residues incorporated by single mutation to form a salt bridge: arginine (blue), aspartic or glutamic acid (red), lysine (cyan). Positive and negative controls are shown in yellow and green respectively. Shadowed points are the three leftmost comparisons for each mutant (lowest RMSD, the most similar mutant to wt structures) and they are shown isolated in Fig. 8. Also, empty points represent comparisons between clusters but respect to others of the same mutant instead of comparing to wildtype clusters (see text). Right. Energy and structural differences for each mutant were averaged from data shown at left. Error bars correspond to one standard deviation from the mean. From top to bottom, the results display runs at A) 298.15, B) 323.15 and C) 348.15 K, respectively.

or subunit dissociation [68]. This report is in clear agreement with our comparative results between the punctual charge of the amino group of the lysine side chain and the resonant dispersed charge in the guanidinium group in arginine. Water seems to compete for the electric charge more in lysine than in arginine (Supplementary Fig. S11). Our MD simulations also show that surface arginine side-chains are better contributors to stability. This differential behavior has been reported before in experimental studies where arginine residues are preferred [67]. Also, genomic studies have demonstrated that salt bridges formed with arginine are preferred in most cases to generate thermostable enzymes [69]. Nevertheless, there are also some reports where the introduction of a lysine residue in a specific site of laccase is better than arginine in the same position [69–73], so generalization has some exceptions.

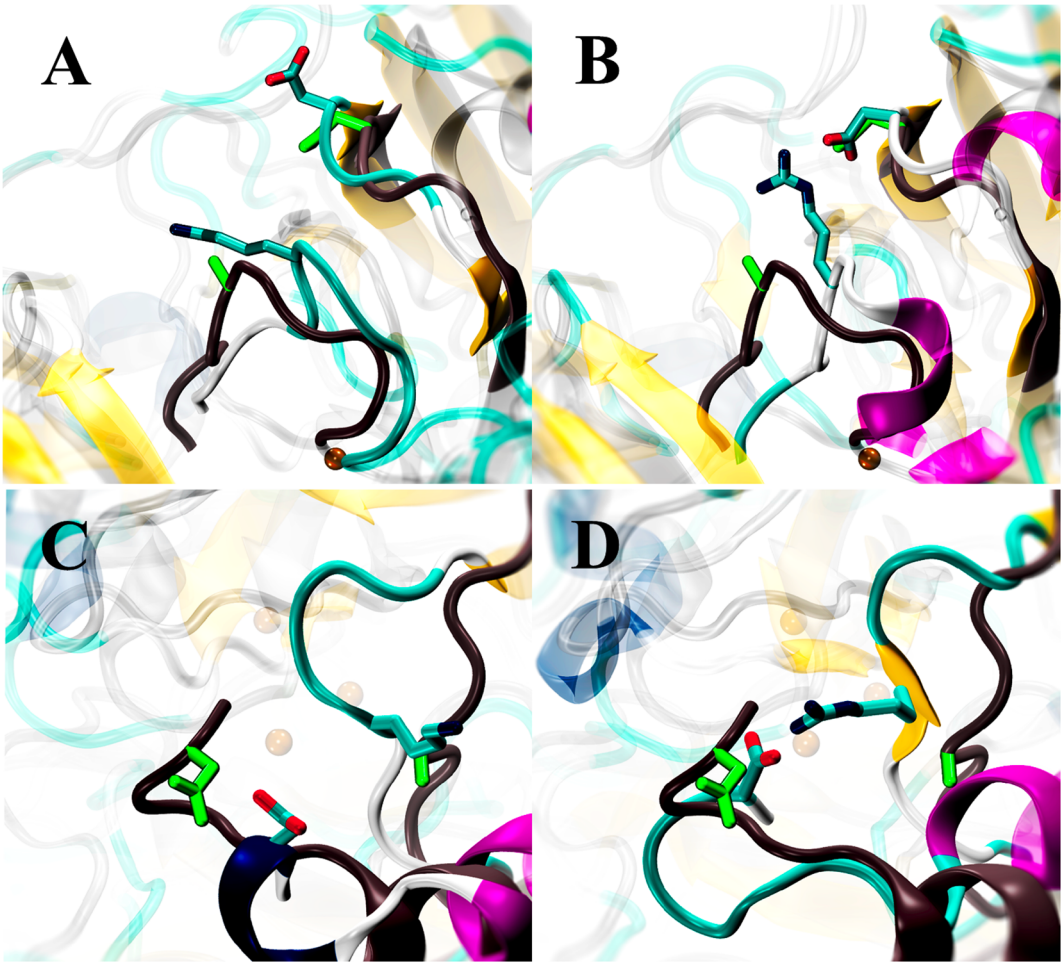

Fig. 7. Arginine compared to lysine in the same salt bridge. A. A71K mutant compared to wildtype structure from representative clusters of MD simulations. B. A71R mutant also compared to its wildtype structure. Distances (averaged on archetypal structures of each cluster) between positive and negative formal charges are 9.1 ± 1.0 and 3.8 ± 0.3 Å, respectively. Ribbons in each panel represent the backbone of mutant (blue) and wildtype (black) structures; green side chains correspond to wildtype. C and D. Comparison of A88K and A88R, similar to those of panel A. Distances between formal charges are in this case are 9.4 ± 1.0 for lysine and 4.3 ± 0.2 Å for arginine respectively.

3.6. Comparison of the same structures in wtTv

As another internal validation of our MD data, each cluster for a particular structure (mutant or wildtype) was compared against the rest of the clusters for the same structure. In Fig. 6 left, these data are presented as empty points. For the sake of simplicity, only data from both wildtype structures and H62R, A88R and A88K mutants are shown, but they are representative of behaviors of the whole set of comparisons. The set of empty points at energy-difference values near to zero circled at the left of Fig. 6, corresponding to the cluster comparison of a structure with respect to the rest of the clusters of the same MD run. As expected, all cluster-representative structures compared are similar, as is reflected by low RMSD values. The energy differences are small when compared to the rest of the points in the picture, meaning that no strong fluctuations are found inside the same MD run, in agreement with data from Fig. 4. Other empty points can be found dispersed in the graph, where they also correspond to cluster comparisons of the same wt or mutant structure but in this case from different MD runs. For example, those circled in the middle of the graph. Again, energies are typically low respect to mutant-wt comparisons (filled points) but somewhat higher than those from the same MD run. The same result is found with their RMSD values, since variability in the structure is a consequence of different seeds and initial velocities in each triplicate simulation, which makes each simulation unique. During the length of the simulations, each run visits different nearby parts of the conformational space. The use of clustering allows identifying representative or archetypal structures for each region of the conformational space and reduces noise from structural and energetic fluctuations inside the cluster. From the analysis of all these empty- and filled-points in Fig. 6 we can state that despite fluctuations in an MD simulation run, or among their triplicates, differences in energy between mutant and wildtype structures are higher and thus significant. Moreover, structural divergence caused by mutations is moderate or similar to that observed for clusters from the same species, except for points above 3 Å, where no empty symbols are found. These latter points correspond to the significant effect of the disruption of a salt bridge in the negative control (green) and for most of the salt bridges introduced with lysine side chains (cyan).

3.7. Effect of temperature

When these scatter diagrams (Fig. 6) are compared at the three different temperatures studied in the MD runs, a similar grouping of data is obtained. This qualitative similarity concedes high robustness to our methodology since each temperature corresponds to independent simulations of 14 mutants ran by triplicate and 3 wildtype structures (two laccases and one β-glucosidase) also ran three times. Again, the snapshots of the last 5 ns of every mutant runs were clustered and compared respect to wildtype clusters. Averaged RMSD values increase with temperature, while energy tends to be less positive (more stabilizing) in agreement with the proposals of Jelesarov et al. [71].

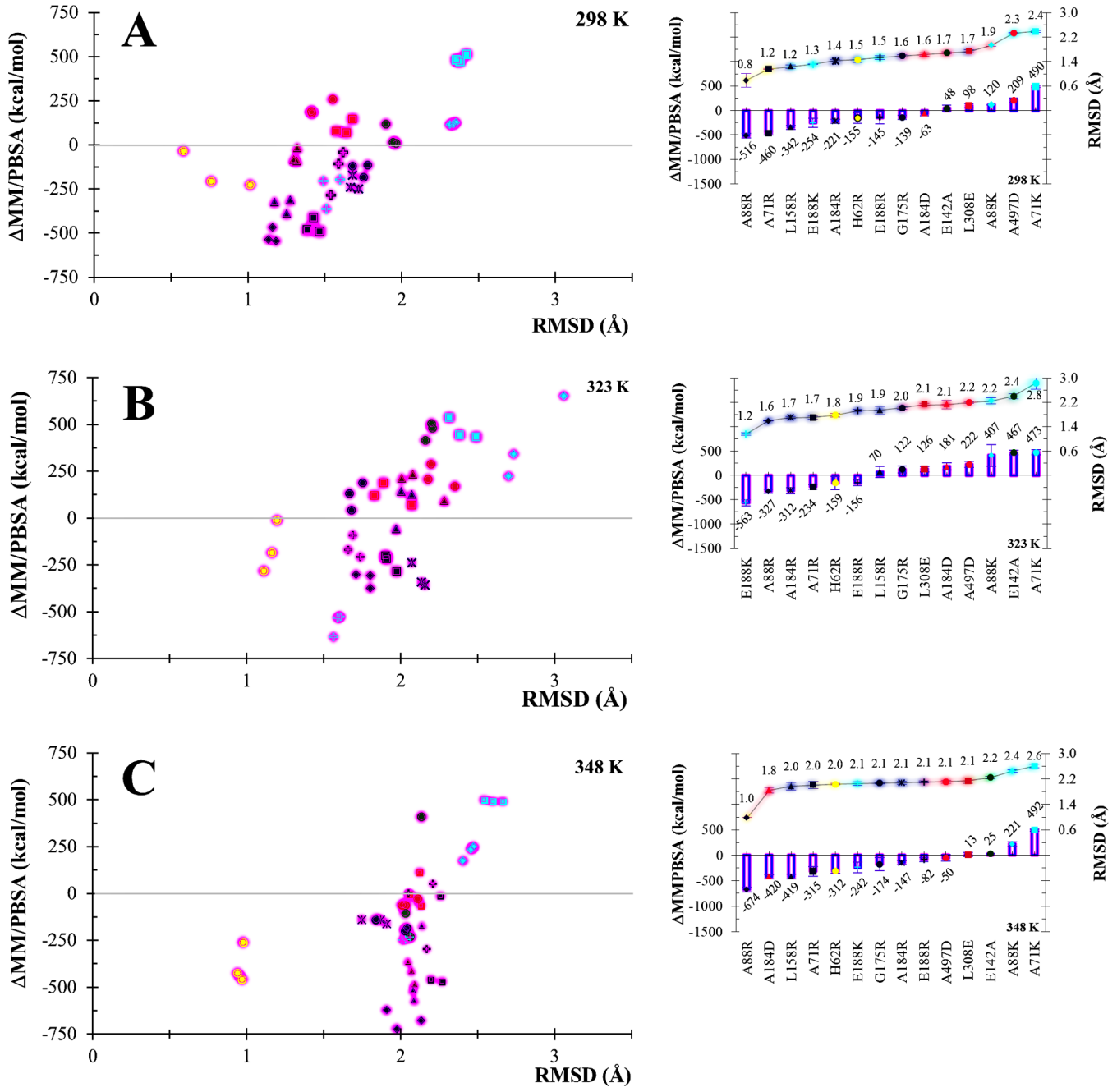

Fig. 8. Comparison of clusters of mutants most structurally similar to their wildtype. Only the three points with the lowest RMS from each mutant-wt comparison are shown. Averages at right were recalculated for the reduced set of points.

3.8. Structurally similar clusters

Fig. 8 presents a data subset of Fig. 6 showing only the mutant clusters with structures more similar to those of their wild-type (subset data collection is available in the Supplementary Table S7). This means that from comparisons of every cluster of each mutant respect to all their wildtype clusters, only the three with the lowest RMS values are presented (leftmost of the whole set of mutant-wildtype clusters). The rationale is to study mutant-wt differences only from the most similar conformations, thus filtering energy differences arising from structural divergence generated during MD simulations. Here the scattering distribution is more evident, showing the points corresponding to the introduced lysine-sidechains even more structurally disturbing and energetically destabilizing than the negative control. Averages at the right of this figure correspond only to the points shown at left. Again the pattern is qualitatively maintained at the three studied temperatures, with higher RMSD values and more negative energies as the temperature increases. Interestingly, the three salt bridges introduced with an acid residue (red) show a neutral or slightly disruptive effect both in energy and in structure, with intermediate positions in diagrams of Figs. 6 and 8 respect to arginine and lysine mutants.

4. Conclusions

Laccase was a good test case in the search for stability determinants due to its modular structure composed of three relatively stable domains. They are associated to form the active structure, with three out of four copper ions in the interdomain regions. These characteristics allowed us to propose and test the stabilizing effect of interdomain salt bridges. The laccase viewed in this modular form is an excellent model

to approach the understanding of the quaternary structural stabilization.

The methodology proposed here showed to be precise to detect and locate positive and negative controls in extreme positions as shown in Figs. 6 and 8. Also, the procedure demonstrated was robust, since triplicated runs yielded consistent results, as well as the independent simulations, ran at three different temperatures.

Concerning laccase, it is interesting to note that it is possible to stabilize its structure with a single mutation forming an interdomain salt bridge, as the cases of A71R or A88R. However, not every interdomain salt bridge succeeded to stabilize the structure. Interestingly, mutations in the same site but introducing a different basic side chain, lysine instead of arginine, showed an opposed effect on stability in wt*Tv*, as discussed in other reports of experimental and theoretical studies [73]. On the other hand, we determined that energy estimations form simple Coulombic electrostatics model is not sufficient to analyze the salt bridge effects. We found that models like PBSA are required for proper electrostatic energy estimation.

Molecular dynamics simulations are a powerful tool for structural studies, like in the study of introducing potential stabilizing contacts. Nevertheless, geometrical fluctuations intrinsic to this technique may mask some comparative analyses like those of a single mutant with respect to its wildtype structure. To surpass this inconvenience, structure classification by clustering proved to be a plausible solution to filter fluctuations from some outlier snapshots and to assemble sets of similar conformers. We did not include in our calculations any entropic estimation from single mutant structures with respect to their wt structures. These estimations augment the dispersion of results and are small enough (about 10–20 kcal/mol) to be disregarded. Also, care must be taken when analyzing multiple mutant systems or small proteins, since a significant change in the number of atoms between mutant and wt structures might introduce considerable errors.

In this work, we proposed and evaluated different interdomain salt bridges designed with the aim to stabilize the structure of *T. versicolor* laccase. A computational protocol of MD simulations was generated and tested by triplicate runs and at three different temperatures. Comparison of results between mutants and their corresponding wildtype structures revealed a diversity of effects in the set of 10 mutants proposed, two of them consistently demonstrated to be stabilizing. It was clear that the Poisson-Boltzmann estimation of electrostatics is preferred over Coulombic models for the utility of clustering for the internal classification of structures in an MD simulation run. Our work not only proposes some thermostable mutants of wt*Tv*, but presents a methodology developed that can be employed to further explore the effect on the stability of new single or multiple mutants in laccases from different species, and the additive or synergic effects of the interaction of mutations inside a structure. Also, it can be used in other multi-domain enzymes and even to be extrapolated to explore stabilization between chains constituting oligomeric biomolecules.

Acknowledgements

The authors gratefully acknowledge the computing time granted by LANCAD and CONACyT on the supercomputer Yoltla at LSVP UAM-Iztapalapa. We wish to thank the Consejo Nacional de Ciencia y Tecnología (CONACyT), Consejo Mexiquense de Ciencia y Tecnología (COMECyT) and Programa para el Desarrollo Profesional Docente para el Tipo Superior (PRODEP, SEP) for supporting this research and providing graduate scholarships.

Conflict of interest statement

The authors report no conflicts of interest in this work.

Appendix A. Supplementary data

Supplementary data to this article can be found online at https://doi.org/10.1016/j.chemphys.2018.10.019.

References

[1] X.X. Zhou, Y.B. Wang, Y.J. Pan, W.F. Li, Differences in amino acids composition and coupling patterns between mesophilic and thermophilic proteins, Amino Acids 34 (2008) 25–33, https://doi.org/10.1007/s00726-007-0589-x.
[2] C. Vieille, G.J. Zeikus, Hyperthermophilic enzymes: sources, uses, and molecular mechanisms for thermostability, Microbiol. Mol. Biol. Rev. 65 (2001) 1–43, https://doi.org/10.1128/MMBR.65.1.1-43.2001.
[3] J. Chen, W.E. Stites, Packing is a key selection factor in the evolution of protein hydrophobic cores, Biochemistry 40 (2001) 15280–15289, https://doi.org/10.1021/bi011776v.
[4] N.J. Christensen, K.P. Kepp, Stability mechanisms of a thermophilic laccase probed by molecular dynamics, PLoS One 8 (2013) e61985, https://doi.org/10.1371/journal.pone.0061985.
[5] I. Matsui, K. Harata, Implication for buried polar contacts and ion pairs in hyperthermostable enzymes, FEBS J. 274 (2007) 4012–4022, https://doi.org/10.1111/j.1742-4658.2007.05956.x.
[6] W.F. Li, X.X. Zhou, P. Lu, Structural features of thermozymes, Biotechnol. Adv. 23 (2005) 271–281, https://doi.org/10.1016/j.biotechadv.2005.01.002.
[7] S. Radestock, H. Gohlke, Protein rigidity and thermophilic adaptation, Proteins 79 (2011) 1089–1108, https://doi.org/10.1002/prot.22946.
[8] P.C. Rathi, S. Radestock, H. Gohlke, Thermostabilizing mutations preferentially occur at structural weak spots with a high mutation ratio, J. Biotechnol. 159 (2012) 135–144, https://doi.org/10.1016/j.jbiotec.2012.01.027.
[9] B. Sohini, S. Srikanta, Turning a mesophilic protein into a thermophilic one: a computational approach based on 3D structural features, J. Chem. Inf. Model. 49 (2009) 1741–1750, https://doi.org/10.1021/ci900183m.
[10] S. Kumar, R. Nussinov, How do thermophilic proteins deal with heat? Cell Mol. Life Sci 58 (2001) 1216–1233, https://doi.org/10.1007/PL00000935.
[11] J.H. Missimer, M.O. Steinmetz, R. Baron, F.K. Winkler, R.A. Kammerer, X. Daura, W.F. van Gunsteren, Configurational entropy elucidates the role of salt-bridge networks in protein thermostability, Protein Sci. 16 (2007) 1349–1359, https://doi.org/10.1110/ps.062542907.
[12] A.V. Gribenko, M.M. Patel, J. Liu, S.A. McCallum, C. Wang, G.I. Makhatadze, Rational stabilization of enzymes by computational redesign of surface charge-charge interactions, Proc. Natl. Acad. Sci. U. S. A. 106 (2009) 2601–2606, https://doi.org/10.1073/pnas.0808220106.
[13] X. Huang, D. Gao, C.G. Zhan, Computational design of a thermostable mutant of cocaine esterase via molecular dynamics simulations, Org. Biomol. Chem. 9 (2011) 4138–4143, https://doi.org/10.1039/c0ob00972e.
[14] M.G. Pikkemaat, A.B. Linssen, H.J. Berendsen, D.B. Janssen, Molecular dynamics simulations as a tool for improving protein stability, Protein Eng. 15 (2002) 185–192, https://doi.org/10.1093/protein/15.3.185.
[15] C. Strub, C. Alies, A. Lougarre, C. Ladurantie, J. Czaplicki, D. Fournier, Mutation of exposed hydrophobic amino acids to arginine to increase protein stability, BMC Biochem. 5 (2004) 9, https://doi.org/10.1186/1471-2091-5-9.
[16] H.R. Bosshard, D.N. Marti, I. Jelesarov, Protein stabilization by salt bridges: concepts, experimental approaches and clarification of some misunderstandings, J. Mol. Recognit. 17 (1) (2004) 1–16, https://doi.org/10.1002/jmr.657.
[17] I. Jelesarov, A. Karshikoff, Defining the role of salt bridges in protein stability, Methods Mol. Biol. 490 (2009) 227–260, https://doi.org/10.1007/978-1-59745-367-7_10.
[18] P. Strop, S.L. Mayo, Contribution of surface salt bridges to protein stability, Biochemistry 39 (2000) 1251–1255, https://doi.org/10.1021/bi992257j.
[19] L. Zhang, M. Buck, Molecular simulations of a dynamic protein complex: role of salt-bridges and polar interactions in configurational transitions, Biophys. J. 105 (2013) 2412–2417, https://doi.org/10.1016/j.bpj.2013.09.052.
[20] P. Upadhyay, R. Shrivastava, P.K. Agrawal, Bioprospecting and biotechnological applications of fungal laccase, 3 Biotech 6 (1) (2016) 15, https://doi.org/10.1007/s13205-015-0316-3.
[21] E.N. Prasetyo, S. Semlitsch, G.S. Nyanhongo, Y. Lemmouchi, G.M. Guebit, Laccase oxidation and removal of toxicants released during combustion processes, Chemosphere 144 (2016) 652–660, https://doi.org/10.1016/j.chemosphere.2015.07.082.
[22] D.M. Mate, M. Alcalde, Laccase engineering: from rational design to directed evolution, Biotechnol. Adv. 33 (1) (2015) 25–40, https://doi.org/10.1016/j.biotechadv.2014.12.007.
[23] T. Kudanga, G.S. Nyanhongo, G.M. Guebitz, S. Burton, Potential applications of laccase-mediated coupling and grafting reactions: a review, Enzyme Microb. Technol. 48 (3) (2011) 195–208, https://doi.org/10.1016/j.enzmictec.2010.11.007.
[24] L.I. Ramírez-Cavazos, C. Junghanns, N. Ornelas-Soto, D.L. Cárdenas-Chávez, C. Hernández-Luna, P. Demarche, E. Enaud, R. Garcia-Morales, S.N. Agathos, R. Parra, Purification and characterization of two thermostable laccases from *Pycnoporus sanguineus* and potential role in degradation of endocrine disrupting chemicals, J. Mol. Catal. B: Enzym. 108 (2014) 32–42, https://doi.org/10.1016/j.molcatb.2014.06.006.
[25] J. Polak, A. Jarosz-Wilkołazka, K. Szałapata, M. Grąz, M. Osińska-Jaroszuk, Laccase-mediated synthesis of a phenoxazine compound with antioxidative and dyeing properties-the optimisation process, N. Biotechnol. 33 (2016) 255–262, https://doi.org/10.1016/j.nbt.2015.09.004.
[26] K. Nakamura, T. Kawabata, K. Yura, N. Go, Novel types of two-domain multi-copper oxidases: possible missing links in the evolution, FEBS Lett. 553 (2003) 239–244,

https://doi.org/10.1016/S0014-5793(03)01000-7.
[27] L.G. Rydén, L.T. Hunt, Evolution of protein complexity: the blue copper-containing oxidases and related proteins, J. Mol. Evol. 36 (1993) 41–66, https://doi.org/10.1007/BF02407305.
[28] J. Correa-Basurto, M. Bello, M.C. Rosales-Hernández, M. Hernández-Rodríguez, I. Nicolás-Vázquez, A. Rojo-Domínguez, J.G. Trujillo-Ferrara, R. Miranda, C.A. Flores-Sandoval, QSAR, docking, dynamic simulation and quantum mechanics studies to explore the recognition properties of cholinesterase binding sites, Chem. Biol. Interact. 209 (2014) 1–13, https://doi.org/10.1016/j.cbi.2013.12.001.
[29] Molecular Operating Environment (MOE), 2013.08; Chemical Computing Group ULC, 1010 Sherbrooke St. West, Suite #910, Montreal, QC, Canada, H3A 2R7, 2017, http://www.chemcomp.com.
[30] B. Webb, A. Sali, Comparative protein structure modeling using modeller, Curr. Protocols Bioinf. 54 (2014) 5.6.1–5.6.37, https://doi.org/10.1002/cpbi.3.
[31] T.A. de Beer, K. Berka, J.M. Thornton, R.A. Laskowski, PDBsum additions, Nucl. Acids Res. 42 (2014) D292–D296, https://doi.org/10.1093/nar/gkt940.
[32] J.C. Phillips, R. Braun, W. Wang, J. Gumbart, E. Tajkhorshid, E. Villa, C. Chipot, R.D. Skeel, L. Kalé, K. Schulten, Scalable molecular dynamics with NAMD, J. Comput. Chem. 26 (2005) 1781–1802, https://doi.org/10.1002/jcc.20289.
[33] A.D. MacKerell Jr., D. Bashford, M. Bellott, R.L. Dunbrack Jr., J.D. Evanseck, M.J. Field, S. Fischer, J. Gao, H. Guo, S. Ha, D. Joseph-McCarthy, L. Kuchnir, K. Kuczera, F.T.K. Lau, C. Mattos, S. Michnick, T. Ngo, D.T. Nguyen, B. Prodhom, W.E. Reiher, B. Roux, M. Schlenkrich, J.C. Smith, R. Stote, J. Straub, M. Watanabe, J. Wiórkiewicz-Kuczera, D. Yin, M. Karplus, All-atom empirical potential for molecular modeling and dynamics studies of proteins, J. Phys. Chem. B 102 (1998) 3586–3616, https://doi.org/10.1021/jp973084f.
[34] H.J.C. Berendsen, J.P.M. Postma, W.F. van Gunsteren, A. DiNola, J.R. Haak, Molecular-dynamics with coupling to an external bath, J. Chem. Phys. 81 (1984) 3684–3690, https://doi.org/10.1063/1.448118.
[35] S. Jo, T. Kim, V.G. Iyer, W. Im, CHARMM-GUI: a web-based graphical user interface for CHARMM, J. Comput. Chem. 29 (2008) 1859–1865, https://doi.org/10.1002/jcc.20945.
[36] S. Haider, G.N. Parkinson, S. Neidle, Molecular dynamics and principal components analysis of human telomeric quadruplex multimers, Biophys. J. 95 (1) (2008) 296–311, https://doi.org/10.1529/biophysj.107.120501.
[37] Y. Niu, D. Pan, D. Shi, Q. Bai, H. Liu, X. Yao, Influence of chirality of Crizotinib on Its MTH1 protein inhibitory activity: insight from molecular dynamics simulations and binding free energy calculations, PLoS One 10 (12) (2015) e0145219, https://doi.org/10.1371/journal.pone.0145219.
[38] R. Krishnan, E.B. Walton, K.J. Van Vliet, Characterizing rare-event property distributions via replicate molecular dynamics simulations of proteins, J. Mol. Model. 15 (2009) 1383–1389, https://doi.org/10.1007/s00894-009-0504-3.
[39] F. Fogolari, E. Moroni, M. Wojciechowski, M. Baginski, L. Ragona, H. Molinari, MM/PBSA analysis of molecular dynamics simulations of bovine-lactoglobulin: free energy gradients in conformational transitions? Proteins 59 (2005) 91–103, https://doi.org/10.1002/prot.20384.
[40] V.S. Pande, A.Y. Grosberg, T. Tanaka, Statistical mechanics of simple models of protein folding and design, Biophys. J. 73 (1997) 3192–3210, https://doi.org/10.1016/S0006-3495(97)78345-0.
[41] D. Sitkoff, K.A. Sharp, B. Honig, Accurate calculation of hydration free energies using macroscopic solvent models, J. Phys. Chem. A 98 (1994) 1978–1988, https://doi.org/10.1021/j100058a043.
[42] T. Hou, J. Wang, Y. Li, W. Wang, Assessing the performance of the MM/PBSA and MM/GBSA methods: I. The accuracy of binding free energy calculations based on molecular dynamics simulations, J. Chem. Inf. Model. 51 (2001) 69–82, https://doi.org/10.1021/ci100275a.
[43] B. Kuhn, P.A. Kollman, Binding of a diverse set of ligands to avidin and streptavidin: an accurate quantitative prediction of their relative affinities by a combination of molecular mechanics and continuum solvent models, J. Med. Chem. 43 (2000) 3786–3791, https://doi.org/10.1021/jm000241h.
[44] Y. Liu, J. Strümpfer, P.L. Freddolino, M. Gruebele, K. Schulten, Structural characterization of λ-repressor folding from all-atom molecular dynamics simulations, J. Phys. Chem. Lett. 3 (2012) 1117–1123, https://doi.org/10.1021/jz300017c.
[45] J.C. Jose, P. Chatterjee, N. Sengupta, Cross dimerization of amyloid-β and αsynuclein proteins in aqueous environment: a molecular dynamics simulations study, PLoS One 11 (9) (2014) e106883, , https://doi.org/10.1371/journal.pone.0106883.
[46] N.M. Glykos, Software news and updates. Carma: a molecular dynamics analysis program, J. Comput. Chem 27 (2006) 1765–1768, https://doi.org/10.1002/jcc.20482.
[47] M.A. Balsera, W. Wriggers, Y. Oono, K. Schulten, Principal component analysis and long time protein dynamics, J. Phys. Chem. 100 (7) (1996) 2567–2572, https://doi.org/10.1021/jp9536920.
[48] C.C. David, D.J. Jacobs, Principal component analysis: a method for determining the essential dynamics of proteins, Methods Mol. Biol. 1084 (2014) 193–226, https://doi.org/10.1007/978-1-62703-658-0_11.
[49] M. Mezei, Simulaid: a simulation facilitator and analysis program, J. Comput. Chem. 31 (2010) 2658–2668, https://doi.org/10.1002/jcc.21551.
[50] W. Humphrey, A. Dalke, K.V.M.D. Schulten, Visual molecular dynamics, J. Mol. Graph 14 (1996) 33–38, https://doi.org/10.1016/0263-7855(96)00018-5.
[51] G. Fiorin, M.L. Klein, J. Hénin, Using collective variables to drive molecular dynamics simulations, Mol. Phys. 111 (22–23) (2013) 3345–3362, https://doi.org/10.1080/00268976.2013.813594.
[52] L.W. Ungar, N.F. Scherer, G.A. Voth, Classical molecular dynamics simulation of the photoinduced electron transfer dynamics of plastocyanin, Biophys. J. 72 (1997) 5–17, https://doi.org/10.1016/S0006-3495(97)78642-9.
[53] M. López, O. Loera, M. Guerrero-Olazarán, J.M. Viader-Salvadó, J.A. Gallegos-López, F.J. Fernández, E. Favela-Torres, G. Viniegra-González, Cell growth and *Trametes ver*sicolor laccase production in transformed *Pichia pastoris* cultured by solid-state or submerged fermentations, J. Chem. Technol. Biotechnol. 85 (4) (2010) 435–440, https://doi.org/10.1002/jctb.2306.
[54] I. Sillitoe, T.E. Lewis, A. Cuff, S. Das, P. Ashford, N.L. Dawson, N. Furnham, R.A. Laskowski, D. Lee, J.G. Lees, S. Lehtinen, R.A. Studer, J. Thornton, C.A. Orengo, CATH: comprehensive structural and functional annotations for genome sequences, Nucl. Acids Res. 43 (2015) D376–D381, https://doi.org/10.1093/nar/gku947.
[55] F.J. Enguita, L.O. Martins, A.O. Henriques, M.A. Carrondo, Crystal structure of a bacterial endospore coat component. A laccase with enhanced thermostability properties, J. Biol. Chem. 278 (2003) 19416–19425, https://doi.org/10.1074/jbc.M301251200.
[56] M. Camarillo-Cadena, G. Garza-Ramos, M. Peimbert, J. Polaina, G. Pérez-Hernandez, R.A. Zubillaga, Additive effect of single amino acid replacements on the kinetic stability of β-glucosidase B, Protein J. 31 (2012) 615–622, https://doi.org/10.1007/s10930-012-9445-2.
[57] R.A. Zubillaga, E. García-Hernández, M. Camarillo-Cadena, M. León, J. Polaina, Effect of a new ionic pair on the unfolding activation barrier of beta-glucosidase B, Protein Pept. Lett. 13 (2) (2006) 113–118, https://doi.org/10.2174/092986606775101698.
[58] N. Mollania, K. Khajeh, B. Ranjbar, S. Hosseinkhani, Enhancement of a bacterial laccase thermostability through directed mutagenesis of a surface loop, Enzyme Microb. Technol. 49 (5) (2011) 446–452, https://doi.org/10.1016/j.enzmictec.2011.08.001.
[59] A. Hernandez-Flores, M.J. Almaraz-Barrera, D. Lozano-Amado, J. Correa-Basurto, A. Rojo-Dominguez, E. Luna-Rivera, M. Schnoor, N. Guillen, R. Hernandez-Rivas, M. Vargas, A new nucleocytoplasmic RhoGAP protein contributes to control the pathogenicity of *Entamoeba histolytica* by regulating EhRacC and EhRacD activity, Cell Microbiol. 18 (2016) 1653–1672, https://doi.org/10.1111/cmi.12603.
[60] M. Bello, B. Valderrama, H. Serrano-Posada, E. Rudiño-Piñera, Molecular dynamics of a thermostable multicopper oxidase from Thermus thermophilus HB27: structural differences between the apo and holo forms, PLoS One 7 (7) (2012) e40700, https://doi.org/10.1371/journal.pone.0040700.
[61] Y. Zhang, Y. Ding, Molecular dynamics simulation and bioinformatics study on chloroplast stromal ridge complex from rice (*Oryza sativa* L.), BMC Bioinf. 17 (2016) 28, https://doi.org/10.1186/s12859-016-0877-0.
[62] D.S. Kanibolotsky, O.V. Novosyl'na, C.M. Abbott, B.S. Negrutskii, A.V. El'skaya, Multiple molecular dynamics simulation of the isoforms of human translation elongation factor 1A reveals reversible fluctuations between “open” and “closed” conformations and suggests specific for eEF1A1 affinity for Ca2 + -calmodulin, BMC Struct. Biol. 8 (2008) 4, https://doi.org/10.1186/1472-6807-8-4.
[63] L.M. Espinoza-Fonseca, D. Kast, D.D. Thomas, Molecular dynamics simulations reveal a disorder-to-order transition on phosphorylation of smooth muscle myosin, Biophys. J. 93 (6) (2007) 2083–2090, https://doi.org/10.1529/biophysj.106.095802.
[64] S. Soni, C. Tyagi, A. Grover, S.K. Goswami, Molecular modeling and molecular dynamics simulations based structural analysis of the SG2NA protein variants, BMC Res. Notes 7 (2014) 446, https://doi.org/10.1186/1756-0500-7-446.
[65] K. Suhre, Y.H. Sanejouand, ElNemo: a normal mode web-server for protein movement analysis and the generation of templates for molecular replacement, Nucl. Acids Res. 32 (2004) W610–W614, https://doi.org/10.1093/nar/gkh368.
[66] T.J. Lane, D. Shukla, K.A. Beauchamp, V.S. Pande, To milliseconds and beyond: challenges in the simulation of protein folding, Curr. Opin. Struct. Biol. 23 (2013) 58–65, https://doi.org/10.1016/j.sbi.2012.11.002.
[67] L. Huang, Y. Liu, X. Liu, L. Ban, Y. Wang, M. Li, F. Lu, Functional expression of *Trametes versicolor* thermotolerant laccase variant in *Pichia pastoris*, Biotechnol. Biotechnol. Equip. 30 (2016) 261–269, https://doi.org/10.1080/13102818.2015.1134278.
[68] H. Zoe, H. Helena, A.M. Joseph, A.T. Sarah, V.R. Carol, The role of salt bridges, charge density, and subunit flexibility in determining disassembly routes of protein complexes, Structure 21 (2013) 1325–1337, https://doi.org/10.1016/j.str.2013.06.004.
[69] N.T. Mrabet, A. Van den Broeck, I. Van den Brande, P. Stanssens, Y. Laroche, A.M. Lambeir, G. Matthijssens, J. Jenkins, M. Chiadmi, H. van Tilbeurgh, F. Rey, J. Janin, W.J. Quax, I. Lasters, M. De Maeyer, S.J. Wodak, Arginine residues as stabilizing elements in proteins, Biochemistry 31 (1992) 2239–2253, https://doi.org/10.1021/bi00123a005.
[70] M. Matsutani, H. Hirakawa, M. Nishikura, W. Soemphol, I.A. Ali, T. Yakushi, K. Matsushita, Increased number of Arginine-based salt bridges contributes to the thermotolerance of thermotolerant acetic acid bacteria, *Acetobacter tropicalis* SKU1100, Biochem. Biophys. Res. Commun. 409 (1) (2011) 120–124, https://doi.org/10.1016/j.bbrc.2011.04.126.
[71] I. Jelesarov, A. Karshikoff, Defining the role of salt bridges in protein stability, Methods Mol. Biol. 490 (2009) 227–260, https://doi.org/10.1007/978-1-59745-367-7_10.
[72] J. Polak, A. Jarosz-Wilkolazka, Structure/redox potential relationship of simple organic compounds as potential precursors of dyes for laccase-mediated transformation, Biotechnol. Prog. 28 (1) (2012) 93–102, https://doi.org/10.1002/btpr.713.
[73] S. Sokalingam, G. Raghunathan, N. Soundrarajan, A study on the effect of surface lysine to arginine mutagenesis on protein stability and structure using green fluorescent protein, PLoS One 7 (7) (2012) e40410, https://doi.org/10.1371/journal.pone.0040410.